

EFFECT OF HYDROGEN ON SURFACE TEXTURING AND CRYSTALLIZATION ON A-SI:H THIN FILM IRRADIATED BY EXCIMER LASER

Paper M904

Hongliang Wang¹, Fernando Lusquiños², Y. Lawrence Yao¹

¹Department of Mechanical Engineering, Columbia University, New York, NY, USA 10027

²Department of Applied Physics, University of Vigo, Vigo, Spain 36200

Abstract

Hydrogenated amorphous silicon (a-Si:H) thin films have been considered for use in solar cell applications because of their significantly reduced cost compared to crystalline bulk silicon, however, their overall efficiency and stability are less than that of their bulk crystalline counterparts. Limited work has been performed on simultaneously solving the efficiency and stability issues of a-Si:H. Surface texturing and crystallization on a-Si:H thin film can be achieved through a one-step laser processing, which can potentially alleviate the disadvantages of a-Si:H in solar cell applications. In this study, hydrogenated and dehydrogenated amorphous silicon thin films deposited on glass substrates were irradiated by KrF excimer laser pulses and the effect of hydrogen on surface morphologies and microstructures are discussed. The sharp micrometer spikes are only fabricated on a-Si:H surfaces, and the large-grained and fine-grained regions caused by two crystallization processes are also induced by hydrogen. Enhanced light absorptance is observed due to light trapping based on surface geometry changes of a-Si:H films, while the formation of a mixture of nanocrystalline silicon and remained a-Si:H after crystallization suggests that the overall material stability can potentially be increased. The relationship between crystallinity, fluence and number of pulses is also investigated. Furthermore, a step-by-step crystallization process is introduced to protect the hydrogen diffusing out in order to reduce the defect density, and the relationship between residue hydrogen concentration, fluence and step width is discussed. Finally, the combined effects show that the one-step process of surface texturing and step-by-step crystallization induced by excimer laser processing is very promising for a-Si:H thin film solar cell applications.

Introduction

Many industrial solar cells in use today use bulk materials as absorbers with crystalline silicon being the

most prevalent. However, crystalline silicon suffers from the disadvantage of high material cost since relatively large thicknesses are required primarily due to its low absorption coefficient. Recently, thin film absorbers are becoming more and more attractive based on their potential for low-cost modules, possibility to create tandem junctions and large-scale manufacturability [1-2]. a-Si:H is the most popular material for use in thin film form due to its low energy economy (cost/watt). The main issue with a-Si:H is the high order of dangling bonds which act as recombination centers that severely reduce the carrier lifetime which results in the solar cell efficiency being below 10%. Additionally, this initial efficiency will decrease by 50% or more when exposed to sunlight over a period of months which is known as the Staebler-Wronski effect or SWE [3].

Due to their low efficiency and instability, thin-film a-Si:H solar cells require a highly efficient light-trapping design to absorb a significant fraction of the incident sunlight and material property changes to increase stability against the SWE. Antireflection (AR) coatings and front-side texturing through the use of alkaline-based solutions, such as KOH and NaOH etching have been used on crystalline silicon solar cells, and pulsed laser irradiation has been used to enhance light trapping on both amorphous and crystalline materials [4-7], however, AR coating requires additional material and anisotropic wet chemical etching is not applicable for amorphous materials or thin films. In addition, in order to reduce the SWE, hybrid a-Si/nc-Si (nanocrystalline silicon) tandem modules have been developed and are able to achieve both higher efficiency and stability compared with single junction a-Si:H [8] due to the use of a thinner a-Si layer and the wider spectral absorption of nc-Si. To eliminate the need for two separate deposition steps which are required to form these tandem cells, laser-induced crystallization of a-Si:H has been proposed to produce a mixture of nc-Si:H and a-Si:H and simultaneously form a light trapping texture on the surface of the material [7]. Therefore, laser-based treatment of a-Si:H may solve its efficiency and stability issues in a one-

step process, which is a promising methodology for thin-film solar cell fabrication.

Extensive work on surface texturing of crystalline bulk silicon had been reported by using both femtosecond and nanosecond laser [9-10]. Wang, et al. [11-12] and Nayak, et al. [7] also achieved both surface texturing and crystallization on a-Si:H thin films by using femtosecond laser. Compared to the femtosecond laser, nanosecond laser can induce more crystallinity due to the longer pulse duration and more thermal effect, which can potentially increase the stability. Therefore, the feasibility of nanosecond laser-induced surface texturing and crystallization of a-Si:H becomes interesting. Many research group focused on excimer laser induced crystallization on non- or low-hydrogen a-Si thin films [13], and Mathe, et al. [14] reported the effect of hydrogen on surface roughness and crystallization of a-Si:H thin films by single pulse irradiation of excimer laser. However, there is no work showing a sharp spiked surface on the a-Si:H thin film after multiple excimer laser pulses irradiation, and how hydrogen plays a role on the laser-induced surface texturing and crystallization is still not very clear.

In this paper, the formation of a densely packed, spiked surface structure has been studied through scanning electron microscopy (SEM) and atomic force microscopy (AFM) for excimer laser irradiation of a-Si:H thin films, and light absorptance dependence of surface structure is studied by spectrophotometry. The time-resolved analysis of melting and solidification of a-Si:H sample was analyzed by *in-situ* front-side transient reflectance measurement. The effect of laser processing on crystallinity and microstructure are investigated by x-ray diffractometry (XRD) and transmission electron microscopy (TEM), and the hydrogen concentration is measured by Fourier transform infrared spectroscopy (FTIR). The experimental results show that the hydrogen is necessary for fabricating sharp spikes on a-Si:H thin films, and the combined effects of light trapping by surface structuring and crystallization illustrate a one-step process for potentially enhancing the efficiency and stability of a-Si:H thin film solar cells.

Background

Hydrogen Effect on Nanosecond Laser-induced Surface Texturing on a-Si:H

Mathe, et al. [14] showed that the surface roughness caused by single-pulse irradiation on a-Si:H could be almost two orders of magnitude larger than that of non-hydrogen a-Si, and mentioned that the movement of H₂ gas bubbles generated by the combination of H atoms

and molecules in the ambient medium are responsible for the surface roughness. Since there is no literature shows sharp spikes formed on a-Si:H surface by multiple nanosecond pulses, the authors believe the mechanism of the spike formation on a-Si:H is the combination of surface texturing on non-hydrogen Si and hydrogen movement which improves the texturing behavior. Therefore, it is necessary to understand the formation mechanism of surface texturing on non-hydrogen Si before studying on a-Si:H.

Nanosecond laser can produce micro-conical/column spikes on bulk crystalline silicon (c-Si) surface at the fluence of 1-5J/cm² after a few hundred to thousands of pulses. The mechanism can be divided into two steps: spike initialization and growth. Dehghanpour, et al. [15] believed that the sharp spikes are initially caused by the generation of capillary waves due to the micro-fluid mechanics of the molten layer, and then the periodic bead-like structure is formed as the seed of the final spikes. The development of the spikes is explained on the formation of preferential removal of the material through Vapor-liquid-solid (VLS) mechanism [10]. The silicon-rich vapor generated between the spikes preferentially redeposits on the molten tip of the microcolumns due to high accommodation coefficient of liquid, like the vapor prefers to dissolve into the liquid rather than solid, so that those spikes grow uniformly with the increasing of laser pulses. At the side of the columns, because the increase reflectivity with increasing incident angle, the sides of spikes are not melted or ablated. At last, the spike growth appears to halt when they reach a certain height.

Hydrogen Effect on Crystallization of a-Si:H

Partial crystallization of a-Si:H is helpful to improve the stability, and bigger grains with less grain boundaries are more desirable microstructures since defects and impurities are always located at grain boundaries. Therefore, hydrogen may have some drawbacks on crystallization effect. First, hydrogen could trigger explosive crystallization [13]. When the incident laser energy density is only sufficient to induce partial melting of a-Si layer, explosive crystallization can be observed and converts a-Si into fine-grained polycrystalline Si via a melt-mediated mechanism [16]. The buried liquid layer is at a temperature higher than the melting point of a-Si, while lower than the melting point of c-Si, and propagates deeply into a-Si layer by simultaneously melting of a-Si and solidifying into c-Si. Due to latent heat difference between c-Si and a-Si, the propagation is self-sustaining. There are two different nucleation scenarios, a moving l-Si/a-Si interface can be unstable

with respect to nucleation of c-Si [17] and small crystallites can nucleate in a-Si during heating phase prior to melting [18], had been made to explain why explosive crystallization occurs. Second, an observation by Mathe, et al. [14] showed that hydrogen slows down the crystallization process because more energy density is needed to crystallize a given depth when hydrogen is present. Large-grained polycrystallites are generated at the hydrogen depletion region near the surface, and fine-grained ones are located at hydrogen contained area underneath.

Therefore, hydrogen could cause fine-grained polycrystallites by explosive crystallization and spend a part of the laser energy that slows down the crystallization process. However, these effects can be alleviated by multiple-pulse radiation which will be discussed later.

Experimental Setup

Amorphous silicon films were deposited on 0.525mm-thick Corning 1747 glass substrates using plasma enhanced chemical vapor deposition (PECVD). The a-Si:H film was deposited at a rate of 60 Å/s in an hydrogen diluted silane environment at 380°C with a hydrogen atomic concentration of around 20 at %. Film thickness was found to be roughly 1.6 μm through ellipsometry measurements [11]. The a-Si:H films were cleaned with acetone in an ultrasonic cleaner for 5 minutes and then rinsed with methanol and distilled water prior to processing.

Surface texturing and crystallization was carried out using an unpolarized, pulsed KrF excimer laser with a wavelength of 248 nm and pulse duration of 30 ns. After passing through an attenuator, the laser beam is homogenized by a multi-lens homogenizer system and then further shaped as it passes through a photomask. This shape is then demagnified (5X) and focused onto the sample through a projection lens. This results in a homogeneous 1mm×1mm square irradiated spot on the sample surface. The sample was mounted on a three-axis translation stage and irradiated by a different number (1-100) of laser pulses with various fluence (0.15J/cm² to 0.5J/cm²) at a stationary spot, and moved to the adjacent point for the next irradiation until an area of 10mm by 10mm. For the step-by-step process, the condition starts at 0.05 J/cm² and ends at the desired final laser fluences (0.3J/cm² and 0.4J/cm²) using step widths from 0.01J/cm² to 0.08J/cm² and number of pulses of 50 or 100 pulses for each step.

The untreated and treated samples were observed through SEM. Surface roughness and the distribution of spikes in the treated samples were also examined

using an AFM. Crystallinity and material microstructure after laser irradiation are analyzed by XRD and TEM, and the hydrogen concentration is investigated by FTIR. The time-resolved analysis of melting and solidification of a-Si:H sample was analyzed by *in-situ* front-side transient reflectance measurement. The optical transmittance and reflectance of as received and laser treated a-Si:H films were measured by a spectrophotometer over a wavelength range of 250nm-2500nm which corresponds to the main spectral range of solar irradiation [19]. The reflectance (R in %) and transmittance (T in %) are then used to calculate the absorptance (A in %) of the film: $A=100-R-T$.

Results and Discussion

Effect of Hydrogen on Surface Morphology

Surface Topography on Laser Irradiated a-Si:H

Lowndes, et al. [10] showed that the polarized pulsed-laser irradiation on c-Si could cause two different phenomenons: at lower fluence (<1J/cm²), laser-induced periodic surface structures (LIPSS) occurs on the silicon surface; at higher fluence (1 to 5J/cm²), columnar or conical spikes of a few tens of micrometers in height are generated. However, regarding to texturing on a-Si:H thin films, a much lower and narrower processing window is tested in order to not damage or crystallize the entire film. In this study, the amorphous samples are irradiated at stationary locations with lower fluences (0.15 J/cm² to 0.5 J/cm²) and numbers of pulses (1 to 100). A typical result achieved using a fluence of 0.4 J/cm² is shown in Fig. 1. The average spike height and spacing after 1 pulse measured by AFM [11] are 460.8±10.6 nm and 1.637±0.037 μm, respectively, where the variation represents standard deviation. As discussed above, beyond the capillary waves formed by solidifying of the molten layer, hydrogen should play an important role in formation of the spikes. It is showed that the hydrogen atoms combine to form H₂ gas, and then diffuse into the ambient medium and leave the blister regions after laser processing [14]. However, a more complex process could occur, i.e. the combined hydrogen molecules may explode when the laser energy is high enough; afterwards, the released pressure drives the upper liquid silicon to move upward while the surrounding liquid silicon flows to the explosion position. The liquid silicon solidifies before it achieves equilibrium, which forms much higher spikes compared to the dehydrogenated a-Si samples. It is noted that no LIPSS structure is observed after 1 pulses based on SEM image of surface morphology shown in Fig. 1 (a). The reason is that the laser beam is unpolarized, and no interference occurs

because of the random phase change between the incident beam and scattered light. After 5 pulses shown in Fig. 1 (b), the spikes are distributed more uniformly and sparsely. After that, the sharp conical spikes are developed on the formation of preferential removal of the material through VLS mechanism as shown in Fig. 1 (c) of surface morphology after 50 pulses, and the average spike height and spacing are $1.837 \pm 0.0317\mu\text{m}$ and $2.121 \pm 0.035\mu\text{m}$, respectively. Figure 1 (d) shows the high magnification SEM image of the spikes formed after 50 pulses, it can be seen that voids are generated underneath the solidified silicon, which indicates the existence of hydrogen explosion. The spikes are partially protruded $1.426 \pm 0.059\mu\text{m}$ from the original surface which is measured by AFM at the boundary of the irradiation area. It is suggested growth is a dominant spike formation mechanism under ns laser than ablation of femtosecond pulses [9].

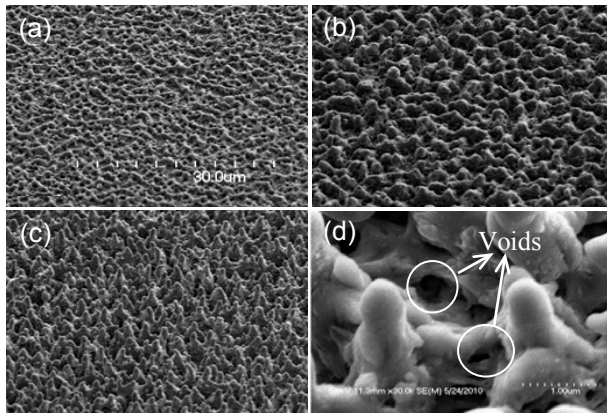


Figure 1. SEM images of a-Si:H film surface after being irradiated by the following number of pulses at $0.4\text{J}/\text{cm}^2$ (a) 1, (b) 5, (c) 50 pulses at the magnification of 1.50K, and (d) 50 pulses at a magnification of 30K

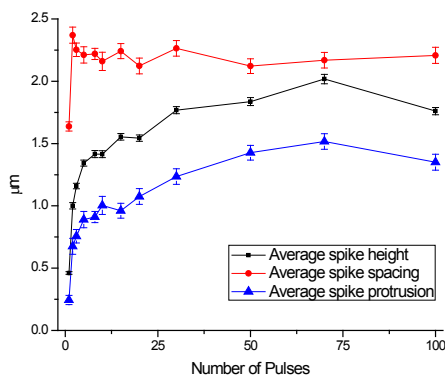


Figure 2. Dependence of average spike height, protrusion and spacing on number of pulses for a fixed fluence of $0.4\text{J}/\text{cm}^2$, determined from an area of $50 \times 50 \mu\text{m}^2$ at the processing center, error bars indicate standard deviation

In order to study the quantitative characteristics of the feature, AFM measurements are performed. The average spike height, protrusion and spacing are measured within an area of $50 \times 50 \mu\text{m}^2$. Figure 2 shows the average spike height, protrusion and spacing correlated with the number of pulses at a fluence of $0.4\text{J}/\text{cm}^2$, and the variation represents standard deviation. It can be divided into 3 regions: first, for the first 10 pulses, the spike height and protrusion are increased rapidly due to the both effects of hydrogen explosion and VLS caused by multiple reflection in between the spikes; second, the from 10 pulses to 70 pulses, the hydrogen are mostly depleted so that the VLS mechanism is dominant, therefore, the average spike height increase rate slows down; third, after 70 pulses, the average spike height increases to around $2\mu\text{m}$, and the silicon-rich ablated material in between the spikes is difficult to achieve to the tips so that VLS cannot happen, the average spike height and protrusion start decreasing. The average spacing remains a constant of around $2.2 \mu\text{m}$ after the first pulse. This is because the molten layer solidifies before being equilibrium at the first pulse and forms a higher tightened surface structure due to the presence of hydrogen, so that the remelting layer by the second pulse cannot be stable. The liquid silicon will be re-distributed due to the surface tension effect and is stabilized until the spike bases are connected together before solidification. After that, the spikes are already initially formed and the following pulses cannot affect the spike spacing any more.

Surface Topography on Dehydrogenated a-Si In order to study the effect of hydrogen on surface morphology, a numerical simulation and experiments of spike formation on laser irradiated dehydrogenated a-Si are investigated to compare with that of a-Si:H samples. For the first pulse, the heat transfer phenomenon can be obtained by Eq. (1) [20],

$$\rho(T)C_p(T)\frac{\partial T(\vec{r},t)}{\partial t} - \nabla[\kappa(T)\nabla(T(\vec{r},t))] = 0 \quad (1)$$

where, ρ , C_p , κ , T , r and t are density, specific heat, thermal conductivity, temperature, radius and time, respectively. The properties of a-Si used in the simulation are collected from references [21-25].

The geometry of the irradiated sample can be considered as semi-infinite. Assuming the sample material is isotropic and uniform, the laser radiation is approximately uniform and the transversal dimension of the irradiated area is larger than the thermal penetration depth, the problem can be considered as a unidimensional model and the temperature field will depend exclusively on the depth (z -axis) [26]. The variation of the thermo-physical parameters (ρ , C_p , κ)

of the a-Si film with the temperature is not big enough to be considered, and average values of these parameters are taken into account. The convection and radiation losses at temperatures between 1000K and 2000K are hardly exceed 1-3 W/cm² [24], so that they are negligible during the simulation. With these hypotheses, Eq. (1) with the initial and boundary conditions can be written as follows:

$$\rho C_p \frac{\partial T(z,t)}{\partial t} - \kappa \nabla^2 [T(z,t)] = 0 \quad (2)$$

$$T(z,t=0) = T_{ambient} \quad (3)$$

$$\kappa \left[\frac{\partial T(z,t)}{\partial z} \right]_{z=0} = Q_{laser} - Q_{ambient} - Q_{radiation} \quad (4)$$

$$\kappa \left[\frac{\partial T(z,t)}{\partial z} \right]_{z=\infty} = 0 \quad (5)$$

where, $Q_{laser} = I(x,y,t)(1-R)q(t)$, and $I(x,y,t)$ is the laser intensity, R is the reflectance and $q(t)$ is the temporal dependence of the laser pulse.

The thermal gradient in the molten pool drives the motion of the liquid silicon provoking the deformation of the surface, and the pressure differences created at a curved interface support the evolution of the deformations on the liquid surface as capillary waves with the dispersion relationship between wave-vector k and angular frequency ω given by [23],

$$\omega^2 = \frac{\alpha k^3}{\rho} \tanh(kh) \quad (6)$$

where, α is the surface tension of the liquid and h is the depth of the molten pool.

In order to obtain the amplitude of the thermo-capillary waves, the Navier-Stokes equation has been solved for a stationary and incompressible fluid stated by the Eq. (7) with the boundary conditions of Eq. (8) and (9),

$$\nabla \bar{v} = 0, \quad \nabla^2 \bar{v} = 0 \quad (7)$$

$$\bar{v} = 0 \text{ at } z = -h \quad (8)$$

$$\eta \left(\frac{\partial v_r}{\partial z} + \frac{\partial v_z}{\partial r} \right) = \frac{\partial \alpha}{\partial r} = \frac{\partial \alpha}{\partial T} \frac{\partial T}{\partial r} \text{ at } z = 0 \quad (9)$$

where \bar{v} is fluid velocity, η is the dynamic viscosity, and the subscripts r and z label the radial and normal components of the velocity, respectively.

Eq. (7) is integrated in z -direction [27] that provides the change in the morphology of the fluid Δz due to the motion of the wave.

$$\Delta z = - \frac{1}{2\eta r} \frac{\partial \alpha}{\partial T} \frac{\partial}{\partial r} \left[r < h^2 > \frac{\partial I}{\partial r} \right] \quad (10)$$

with $I = \int_{T_s > T_m} (T_s - T_m) dt$ and

$< h^2 > I = \int_{T_s > T_m} h^2 (T_s - T_m) dt$, T_s the surface temperature and T_m the melting temperature of a-Si.

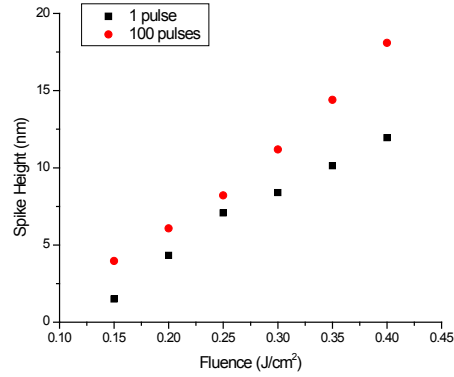


Figure 3. Simulation results of dependence of the spike height on laser fluence for a fixed number of pulses

For multiple pulses, the following hypotheses are established: first, the influence of the phase transformation after the pulses on the thermal and optical properties is negligible; second, the reflectance is only affected by the change of surface roughness. The simulated spike heights at different fluence and number of pulses are shown in Fig. 3. The spike height at 1 or 100 pulses almost linearly increase with increasing of fluence. According to [14], the spike heights at 1 pulse are close to the experimental results. The average spike height of laser irradiated dehydrogenated a-Si thin films (prepared by thermal annealing at 80 hours) at 0.4J/cm² and 100 pulses is around 58nm, and this is also in the same order of magnitude as the simulation result. The numerical predictions are underestimated compared to the spike height obtained experimentally. The reason could be: first, the reflectance is not a constant spatially, i.e. the light absorption inside the valleys is more than that in the peaks. Therefore, more material is actually ablated and redeposited on the tips; second, the material in the simulation is uniform, but in reality, a-Si has a lot of defects and impurities, such as residual hydrogen, these imperfect properties could intense the light absorption and improve the spike height. Therefore, the simulation is valid and reflects that the formation mechanism of dehydrogenated a-Si is reasonable.

In order to show the effect of hydrogen on surface morphology experimentally, the a-Si:H samples are annealed in a vacuumed furnace at 450°C [28] for different time to diffuse out hydrogen as much as

possible. Figure 4 shows the FTIR spectra measured for different annealing time. The non-hydrogen a-Si sample is introduced as a reference spectrum. The hydrogen concentration can be estimated from peaks caused by the stretching mode of Si-H at 2000cm^{-1} and SiH_2 at 2100cm^{-1} using equation [28]:

$$N = A \int \frac{\alpha}{\omega} d\omega = A \frac{S}{t\omega_0} \quad (11)$$

where N , A , α , ω , t , ω_0 , and S are the hydrogen density, the conversion factor ($9 \times 10^9 \text{ cm}^{-2}$ at 2000 cm^{-1} and $2.2 \times 10^{10} \text{ cm}^{-2}$ at 2100 cm^{-1}), the absorbance, the frequency, the film thickness, the peak frequency, and the peak area, respectively.

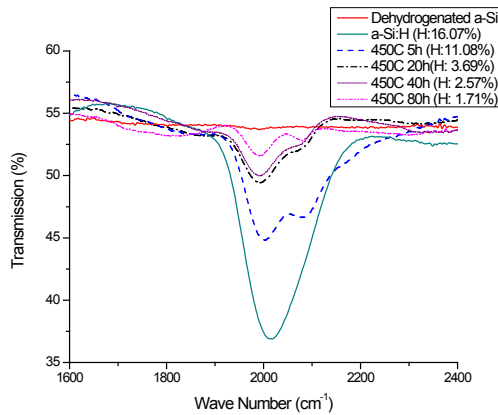


Figure 4. Transmission infrared spectra for thermal annealed a-Si:H samples at different annealing time

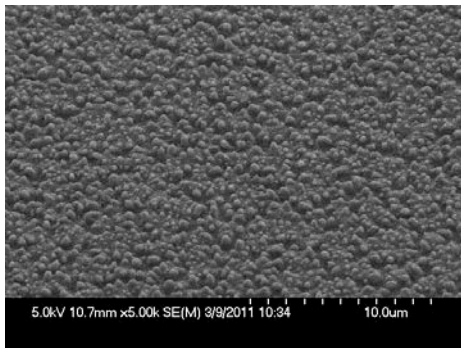


Figure 5. SEM images of 80-hour thermal annealed a-Si:H film after being irradiated at a fluence of $0.4\text{J}/\text{cm}^2$ and 100 pulses, showing no sharp spikes on the surface

Based on Eq. (11), the initial H concentration of 16.07% is highly reduced to 1.71% after thermal annealing after 80 hours, and the XRD measurement shows that the thermal annealed sample still remain amorphous (not shown). The SEM image of laser processed 80-hour-annealed sample at a fluence of $0.4\text{J}/\text{cm}^2$ with 100 pulses is shown in Fig. 5, and the

average spike height is $57.8 \pm 2.15\text{nm}$. It can be seen that no sharp spikes are formed without the help of hydrogen. As discussed above, the molten layer can form capillary waves after solidification, however, the amplitude of the wave is too small to introduce the light multiple reflection towards to the valleys. Therefore, when the next pulse comes, the irradiated area will be melted again similarly as the first pulse and no spikes are formed after multiple pulses. This is different from the femtosecond laser experiments which ablation is dominant, the sharp spikes can be fabricated due to the different ablation rate when the periodic surface structure is formed. Moreover, dehydrogenate a-Si thin films cannot be applied by higher fluences used for c-Si, since it is easy to damage the entire film. Therefore, both the simulation and experiment results show that hydrogen is necessary for forming sharp spikes on a-Si:H thin films.

Effect of Hydrogen on Crystallization and Absorbance

In order to study the crystallization of the treated films, x-ray diffraction patterns were taken for the untreated and treated a-Si:H films are shown in Fig. 6. The spectra have been shifted vertically for clarity. Three peaks at around $2\theta=29^\circ$, 47° and 56° emerge after processing in air which indicate a structural change after laser irradiation and can be indexed to the (111), (220) and (311) crystalline orientations of silicon. The normalized crystallinity is estimated by the calculated area differences of the measured spectra between the laser processed and untreated samples. The largest area at the condition of $0.4\text{J}/\text{cm}^2$ and 100 pulses is defined as a crystallinity of 100%, and the other conditions are calculated by dividing it. The normalized crystallinity at conditions of $0.4\text{J}/\text{cm}^2$ with 50 pulses, and $0.3\text{J}/\text{cm}^2$ with 100 pulses are 98.98% and 57.38%, respectively. It is understood that under partial melting regime, the higher the fluence, the higher the crystallinity. However, under the same fluence, when the number of pulses achieves a certain number, the crystallinity remains the same. This is because the spikes can reach a certain height to avoid the ablated material redepositing to the tips, so that there will no more amorphous material can be melted underneath the crystallized layer.

Hydrogen Effect on Crystallization Single-pulse laser irradiation as well as *in situ* front-side transient reflectance (FTR) measurement are performed for analyzing the dynamics of melting and solidification of a-Si:H thin films. Figure 7 shows the FTR signals correlation with different fluences ($0.1\text{J}/\text{cm}^2$ to $0.5\text{J}/\text{cm}^2$). It can be seen that no damage or phase change at $0.1\text{J}/\text{cm}^2$. The signal intensity decrease at

0.15J/cm² indicates that the material starts being crystallized since the reflectivity of c-Si is lower than that of a-Si. When the fluence is higher than 0.15J/cm², the signal oscillation, due to the interference effect resulting from the fast-moving melting buried layer, shows that explosive crystallization occurs [13] at the beginning. The following plateau means that the solidified surface has been re-melted by the rest of the pulse, and it can be seen that higher fluence always has a longer lifetime of the molten pool, which may cause larger grains after crystallization. Hu, [29] showed that no explosive crystallization occurs for excimer laser irradiated dehydrogenated a-Si deposited by PECVD. Therefore, hydrogen must play a role for triggering explosive crystallization. However, the reason is not clear at this point. It is suggested that the H atom moving may absorb or release the energy and change the temperature in the local area. At some point, nucleation could occur due to the heating or change of the molten Si cooling rate locally, and these nuclei will be the seeds of triggering the explosive crystallization.

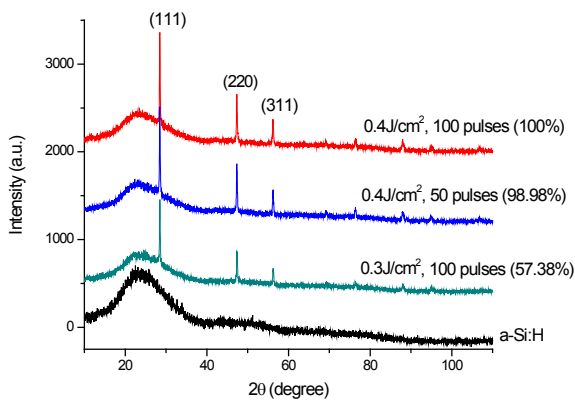


Figure 6. X-ray diffraction spectra of as-received a-Si:H film, laser treated films at 0.4J/cm² with 50 and 100 pulses, and 0.3J/cm² with 100 pulses. The spectra have been shifted for clarity

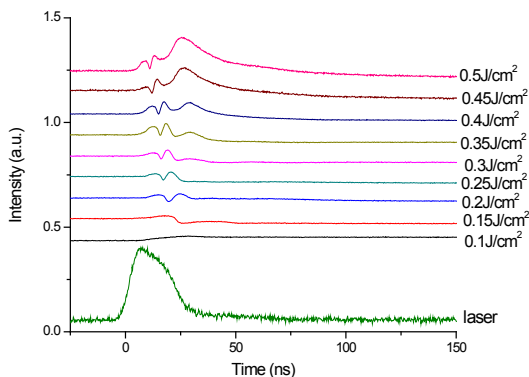


Figure 7. *in-situ* front-side transient reflectance signals of a-Si:H films irradiated at different fluences

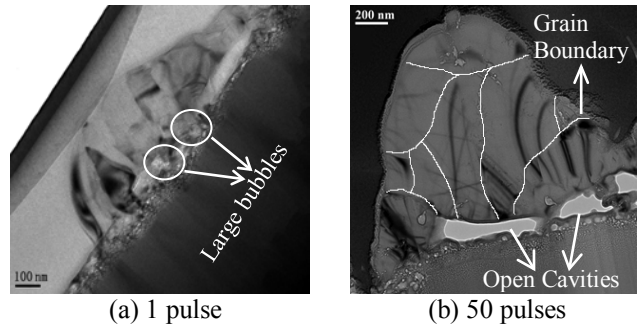


Figure 8. Cross-sectional view TEM micrographs of a-Si:H samples irradiated at (a) 1 and (b) 50 pulses with a fluence of 0.4J/cm²

Figure 8 shows the cross-sectional TEM images at the fluence of 0.4J/cm² with different number of pulses. It can be seen that after the first pulse, microstructure of the material can be divided into two regions – large- and fine-grained regions. The FTIR signal shows that explosive crystallization occurs within 20ns which forms the fine-grained region, and after that, the top layer has been melted again because of the heat accumulation by the rest of the pulse. The hydrogen atoms inside the material start moving by absorbing the laser energy and aggregating at the interface between the solid and liquid silicon. Those hydrogen atoms combine as molecules and form as bubbles, and those bubbles keep dilating and explode when the internal pressure inside the bubbles becomes higher than the outside. The bubble explosion at the liquid/solid silicon interface drives the liquid silicon move up and the surrounding liquid flows towards it. Before the liquid silicon become equilibrium, the material has been solidified and formed as spikes with a height of ~350nm and left large bubbles at the interface as shown in Fig. 8 (a). Because the molten layer at the surface can last for almost 20ns, the crystallized material can form much larger grains of ~140nm than that of explosive crystallization. Figure 8 (b) shows the cross sectional TEM image of a-Si:H sample irradiated at 50 pulses. The connected open cavities underneath the spikes are caused by the hydrogen bubble explosions. In order to estimate the grain size, the TEM sample was tilted with a step of 0.1° in both x and y directions to get avoid the effect of band contours. Since different grain will have different band contours at a certain direction, the moving region of the same contour shows the grain region. It is shown that the large-grained region is only located on the spike and the largest grain size is around 400nm.

Hydrogen Effect on Absorptance The absorptance spectra of untreated and laser treated samples are shown in Fig. 9. It can be seen that the absorptance increases over the entire spectrum. The absorptance spectra of the laser processed samples under different

conditions are similar due to the similar light-trapping surface geometries, and the absorptance at the below-band-gap region could be caused by the impurities and defects generated during the laser processing. It is noted that the absorptance decreases rapidly at the wavelength of $\sim 300\text{nm}$, which may be caused by the interference at the open cavities. As shown in Fig. 8 (b), the depth of the open cavity is around 150nm , and based on the constructive interference equation $2nd = m\lambda$, where n , d , m and λ are refractive index, cavity depth, integer and wavelength. Here, $n=1$ and $d=150\text{nm}$, therefore, the corresponding wavelengths can introduce constructive interference for light reflection are 300nm , 150nm and 100nm , etc. That illustrates the absorptance spectra get the lowest value at around the wavelength of 300nm and will perform periodically while moving to shorter wavelengths.

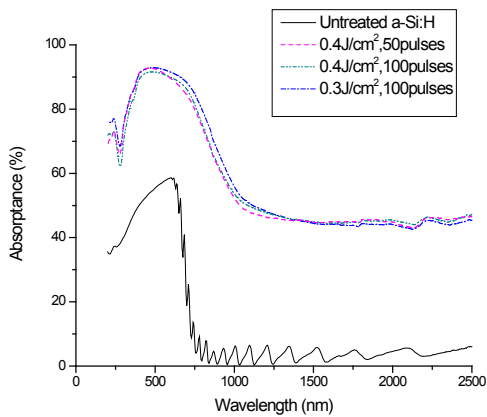


Figure 9. Comparison of absorbance spectra measured by spectrophotometry of as-received and laser irradiated a-Si:H films at fluences of $0.4\text{J}/\text{cm}^2$ with 50 and 100 pulses, and $0.3\text{J}/\text{cm}^2$ with 100 pulses

Effect of Step-by-step Process on Residual Hydrogen Concentration and Crystallinity

Hydrogen is used for passivation of the defects in the Si network and grain boundaries in order to increase the efficiency of the solar cell. However, the FTIR spectra show that there is no hydrogen left after laser processing at the conditions of $0.3\text{J}/\text{cm}^2$ and $0.4\text{J}/\text{cm}^2$ with 100 pulses (not shown). Therefore, leaving as much hydrogen as possible after processing is another criterion. Lengsfeld, et al. [30] shows that a residual hydrogen concentration of $\sim 5\%$ was observed after step-by-step excimer laser induced crystallization of a-Si:H with an initial hydrogen content of 10% .

In this study, step-by-step processes starting at a fluence of $0.05\text{J}/\text{cm}^2$ with a desired final fluence of $0.3\text{J}/\text{cm}^2$ and different step widths from $0.01\text{J}/\text{cm}^2$ to $0.08\text{J}/\text{cm}^2$ are taken, and 100 pulses are used for each

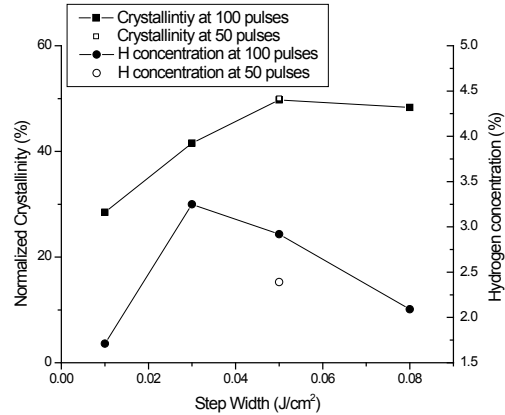


Figure 10. Normalized crystallinity and hydrogen concentration of step-by-step laser processed a-Si:H samples at a final fluence of $0.3\text{J}/\text{cm}^2$ with different step widths and number of pulses

process sequence. The quantitative characteristics of hydrogen concentration and normalized crystallinity based on Eq. (11) and XRD measurement are shown in Fig. 10. For 100 pulses at each step, a maximum hydrogen concentration is achieved at 3.25% with a step width of $0.03\text{J}/\text{cm}^2$. Based on the FTR measurement, the a-Si:H sample starts to be crystallized at $0.15\text{J}/\text{cm}^2$. At the step of $0.01\text{J}/\text{cm}^2$, there are almost 10 steps before the structure phase change. However, the hydrogen inside the material will be diffused out due to the laser-induced thermal effect during those undamaged steps. Therefore, the hydrogen concentration at the step of $0.01\text{J}/\text{cm}^2$ is smaller than that of $0.03\text{J}/\text{cm}^2$. When the step goes to $0.05\text{J}/\text{cm}^2$, thermal annealing by lower fluences is less dominant since only 2 to 3 steps before the crystallization threshold. However, the fluence at each step plays a more important role. Since the crystallized material performs as a protection layer for hydrogen from diffusing out, at the step of $0.03\text{J}/\text{cm}^2$, after the crystallization threshold, the laser pulse at each step is less energetic compared to that of $0.05\text{J}/\text{cm}^2$, which indicates that less energy is transferred underneath the crystallized layer to diffuse out the hydrogen at each step. Although more steps are taken, the final residual hydrogen is still less for the smaller-step process. Likewise, an even lower hydrogen concentration is detected at a step of $0.08\text{J}/\text{cm}^2$. For crystallinity, it can be observed that crystallinity increases with increasing of step width until it achieves $0.05\text{J}/\text{cm}^2$ and keeps at around 50% afterwards. The reason is that with a smaller step, the laser process at each step can only melt a shallower layer compared to that caused by a higher step; therefore, less material can be crystallized after each step. The final crystallinity will become less for smaller-step processed samples although more steps are taken. When the step width reaches higher

than $0.05\text{J}/\text{cm}^2$, the crystallinity remains a constant at around 50%. This is because when the spikes are grown to the saturated height, the ablated material cannot reach to the tips of spikes. Therefore, beyond this point, only remelting and recrystallizing of the crystallized material occur at each step, but no effect on crystallinity. Likewise, at the step of $0.05\text{J}/\text{cm}^2$, the crystallinity is also unchanged at both 50 and 100 pulses at each step. Overall, the condition at the step of $0.05\text{J}/\text{cm}^2$ and 100 pulses may cause a relatively good performance at both cell efficiency and stability.

Figure 11 shows the comparison of absorbance between single-step and step-by-step processed a-Si:H samples. It can be seen that all the laser processed samples perform the same. The inset shows the SEM image of a step-by-step processed a-Si:H sample at a final fluence of $0.3\text{J}/\text{cm}^2$ with a step of $0.05\text{J}/\text{cm}^2$ and 100 pulses at each sequence. A similar formation of spikes is observed compared to the single-step processed sample shown in Fig. 1, which causes a similar absorbance due to the similar change of surface geometry. It is also noted that the interference at around 300nm is not eliminated by step-by-step processes, which means open cavities are still formed as shown in Fig. 8 (b). Overall, the combined effects of surface texturing, crystallization and residual hydrogen by excimer laser-induced step-by-step process of a-Si:H thin films may be ideal for solar cell fabrication.

Conclusion

In conclusion, it has been demonstrated that hydrogen is necessary for the formation of sharp spikes on the surface of a-Si:H thin films irradiated by multiple

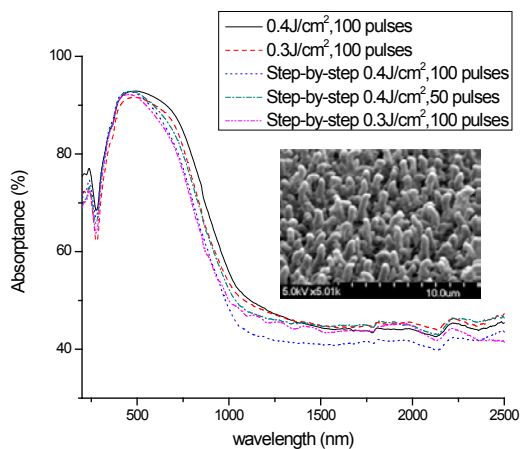


Figure 11. Comparison of absorbance spectra measured by spectrophotometry of single-step and step-by-step laser processed a-Si:H samples, inset shows the SEM image of surface morphology of a step-by-step laser processed a-Si:H sample

excimer laser pulses. Hydrogen can also trigger explosive crystallization at the first 15-20ns, and then crystallized Si on the top will be re-melted in the next tens of nanoseconds. The released pressure by H_2 gas bubble explosion at the interface between liquid and solid Si will drive the liquid Si to move up and form as spikes after solidification. After, the spikes are grown by VLS mechanism until they reach a certain height of $\sim 2\mu\text{m}$ and the crystallinity also saturates at this point because no more amorphous material underneath the crystallized layer can be melted. The large-grain polycrystallites are located on the spikes and fine-grain ones are distributed underneath, with open cavities caused by hydrogen explosion at the interface. Furthermore, laser step-by-step process is taken in order to leave hydrogen as much as possible after processing. It is shown that the residual hydrogen concentration depends on the final fluence, the step width and the number of pulses, and a maximum hydrogen concentration of 3.25% is obtained at a final fluence of $0.3\text{J}/\text{cm}^2$ with steps of $0.03\text{J}/\text{cm}^2$ and 100 pulses for each step. Finally, both single-step and step-by-step processed samples perform a similar absorption capability due to the similar surface geometries obtained after different laser processes. It can be concluded that excimer laser step-by-step processing of a-Si:H thin films may allow for more efficient and stable solar cells.

References

- [1] Luque, A. & Hegedus, S. (2003) Handbook of photovoltaic science and engineering, Wiley, UK, 7-8
- [2] Kazmerski, L.L. (2006) Solar Photovoltaics R&D at the Tipping Point: A 2005 Technology Overview, J. of Elec. Spec. and related Phenomena, 150, 105-135
- [3] Staebler, D.L. & Wronski, C.R. (1980) Optically induced conductivity changes in discharge-produced hydrogenated amorphous silicon, Journal of Applied Physics, 51(6)
- [4] Martirosyan, Kh.S., Hovhannisyan, A.S. & Arouiounian, V.M. (2007) Calculation of reflectance of porous silicon double-layer antireflection coating for silicon solar cells, Physica Status Solidi (C), 4(6), 2103-2106
- [5] Hylton, J.D., Burgers A.R. & Sinke, W.C. (2004) Alkaline etching for reflectance reduction in multicrystalline silicon solar cells, Journal of the Electrochemical Society, 151(6), G408-G427
- [6] Crouch, C.H., Carey, J.E., Warrender, J.M., Aziz, M.J., Mazur, E. & Genin, F.Y. (2004) Comparison of structure and properties of femtosecond and nanosecond laser-structured silicon, Applied Physics Letters, 84(11), 1850-1852

- [7] Nayak, B.K. & Gupta, M.C. (2007) Femtosecond-laser-induced-crystallization and simultaneous formation of light trapping microstructures in thin a-Si:H films, *Appl. Phys. A*, 89, 663-666
- [8] Yamamoto, K., et al. (2004) A high efficiency thin film silicon solar cell and module, *Solar Energy*, 77, 939-949
- [9] Tull, B.R., Carey, J.E., Mazur, E., McDonald, J.P. & Yalisove, S.M. (2006) Silicon surface morphologies after femtosecond laser irradiation, *MRS Bulletin*, 31(8), 626-633
- [10] Lowndes, D.H., Fowlkes, J.D. & Pedraza, A.J. (2000) Early stage of pulsed-laser growth of silicon microcolumns and microcones in air and SF₆, *Applied Surface Science*, 154-155, 647-658
- [11] Wang, H., Kongsuwan, P., Satoh, G. & Yao, Y.L. Femtosecond laser-induced simultaneous surface texturing and crystallization of a-Si:H thin film. Part I: Experiment and morphology study, *Journal of Manufacturing Science and Engineering*, under review
- [12] Wang, H., Kongsuwan, P., Satoh, G. & Yao, Y.L. Femtosecond laser-induced simultaneous surface texturing and crystallization of a-Si:H thin film. Part II: Absorption and crystallinity, *Journal of Manufacturing Science and Engineering*, under review
- [13] Im, J., Kim, H. & Thompson, M. (1993) Phase transformation mechanisms involved in excimer laser crystallization of amorphous silicon films, *Applied Physics Letter*, 63(14), 1969-1971
- [14] Mathe, E., Naudon, A., Elliq, M., Fogarassy, E. & Unamuno, S. (1992) Influence of hydrogen on the structure and surface morphology of pulsed ArF excimer laser crystallized amorphous silicon thin films, *Applied Surface Science*, 54, 392-400
- [15] Dehghanpour, H., Parvin, P., Sajad, B. & Nour-Azar, S. (2009) Dose and pressure dependence of silicon microstructure in SF₆ gas due to excimer laser irradiation, *Applied Surface Science*, 255, 4664-4669
- [16] Polman, A., Roorda, S., Stolk, P. & Sinke, W. (1991) Triggering explosive crystallization of amorphous Silicon, *Journal of Crystal Growth*, 108, 114-120
- [17] Tsao, J. & Peercy, P. (1987) Crystallization instability at the amorphous-silicon/liquid-silicon interface, *Physical Review Letters*, 58(26), 2782-2785
- [18] Roorda, S. & Sinke, W. (1989) Rapid nucleation in pulsed laser heated amorphous Si, *Applied Surface Science*, 36, 588-596
- [19] Goetzberger, A., Knobloch, J. & Voss, B. (1998) *Crystalline silicon solar cells*, Wiley, Chichester, 2
- [20] Carslaw, H.S. & Jaeger J.C. (1958) *Conduction of Heat in Solids*, 2nd Edition, Oxford Univ. Press, 10pp.
- [21] Unamuno, S. & Fogarassy, E. (1989) A thermal description of the melting of c- and a-Silicon under pulsed excimer lasers", *Appl. Surface Sci.*, 36, 1-11
- [22] Ong, C.K., Sin, E.H. & Tan, H.S. (1986) Heat-flow calculation of pulsed excimer ultraviolet laser's melting of amorphous and crystalline silicon surfaces, *J. Opt., Soc. Am. B*, 3(5), 812-814
- [23] Kolasinski, K.W. (2007) Solid structure formation during the liquid/solid phase transition", *Current Opinion in Solid State and Material Science*, 11, 76-85
- [24] Bäuerle, D. (2000) *Laser Processing and Chemistry*, 3rd Edition, Springer, 105pp.
- [25] Ong, C.K., Tan, H.S. & Sin, E.H. (1986) Calculations of melting threshold energies of crystalline and amorphous materials due to pulsed-laser irradiation, *Materials Sci. and Engi.*, 79, 79-85
- [26] Prokhorov, A.M., Konov, V.I. & Ursu, I. (1990) *Laser Heating of Metals*, Taylor and Francis, 43pp.
- [27] Schwarz-Selinger, T., Cahill, D.G., Chen, S., Moon, S. & Griogoropoulos, C.P. (2001) Micron-scale modifications of Si surface morphology by pulsed-laser texturing", *Physical Review B*, 64, 155323-1-7
- [28] Heya, A., Serikawa, T., Kawamoto, N. & Matsuo, N. (2008) Behavior of hydrogen in excimer laser annealing of hydrogen-modulation-doped amorphous silicon layer", *Jap. J. of Appl. Phys.*, 47(3), 1853-1857
- [29] Hu, Q. (2010) Dynamics of Melt-mediated Crystallization of Amorphous Silicon Films, Ph.D thesis, Columbia University
- [30] Lengsfeld, P., Nickel, N. & Fuhs, W. (2000) Step-by-step excimer laser induced crystallization of a-Si:H, *Applied Physics Letters*, 76(13), 1680-1682

Meet the Authors

Hongliang Wang received his M.S. from Harbin Institute of Technology, China. He is currently a doctoral student at the Manufacturing Research Laboratory at Columbia University.

Dr. Fernando Lusquiños is an Associate Professor in the Department of Applied Physics at University of Vigo, Spain. He received his Ph.D. from Vigo University in 2001.

Dr. Y. Lawrence Yao is a Professor in the Department of Mechanical Engineering and director of Manufacturing Research Laboratory at Columbia University. He received his Ph.D. from the University of Wisconsin-Madison in 1988.